Results in Engineering 21 (2024) 101805

Contents lists available at ScienceDirect

Results in Engineering

journal homepage: www.sciencedirect.com/journal/results-in-engineering

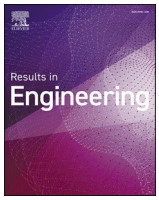

Kirigami-inspired gas sensors for strain-insensitive operation

Jeonhyeong Park [a], Hyeoncheol Lim [a], Junwoo Yea [a], Chaehyun Ryu [a], Soon In Jung [a], Runia Jana [a], Kyung-In Jang [a], Hohyun Keum [b,**], Hoe Joon Kim [a,*]

[a] Department of Robotics and Mechatronics Engineering, Daegu Gyeongbuk Institute of Science & Technology (DGIST), Daegu, 42988, South Korea
[b] Digital Health Care R&D Department, Korea Institute of Industrial Technology (KITECH), Cheonan, 31056, South Korea

ARTICLE INFO

Keywords:
Kirigami
Gas sensor
Flexible
Functionalization

ABSTRACT

Wearable electronics for the Internet of Things (IoT) have spurred interest in optimizing stretchable substrates, electrodes, and sensing materials. Specifically, wearable gas sensors are valuable for real-time monitoring of hazardous chemicals. For wearable gas sensors, a stable operation under mechanical deformation is required. Here, we introduce strain-insensitive Kirigami-structured gas sensors decorated with titanium dioxide (TiO_2) functionalized carbon nanotubes (CNTs) for NO_2 sensing. The Kirigami-shaped substrate is used to ensure mechanical stability when stretched. The developed device shows only a 1.3 % change in base resistance under 80 % strain. In addition, the impact of electro-thermal properties at various strain levels is analyzed to aid the understanding of the device's performance. The CNT-TiO_2 composite induced alterations in p-n heterojunctions, improving the measurement sensitivity by approximately 250 % compared to a bare CNT sensor. Additionally, the sensors exhibited a 10-fold faster desorption rate due to the enhanced photocatalytic effect of TiO_2 under UV exposure. Remarkably, the Kirigami-structured gas sensors maintained stable and repetitive sensing operation even under 80 % strain, which would be enough to be used in various wearable applications.

1. Introduction

The emergence of the Internet of Things (IoT) has brought advancement in wearable technologies owing to applicability in daily life. In particular, there is growing attention towards environmental and industrial fields as wearable technologies allow real-time onsite monitoring of various safety-related parameters [1–3]. Specifically, wearable chemical sensors play a part in various forms, such as smart clothes, eyeglasses, and electronic skins [1], for leakage monitoring of harmful gases to identify workplace hazards. Advanced wearable gas sensors should have flexibility, stretchability, and respectful sensing performances.

Polymeric substrates have been widely used for wearable gas sensors as they are flexible, stretchable, and low-cost [4]. Furthermore, elastomeric substrates, like polydimethylsiloxane (PDMS) and Ecoflex, are biocompatible, enabling them to be interfaced with either human skins or body-worn textiles [5–10]. Paper substrates can also be utilized as they are eco-friendly and lightweight [11]. However, various fabrication methods, such as spin coating, drop-casting, and vacuum filtration, should be considered due to the high surface roughness and porosity of paper substrates [12–14]. In general, the mechanical properties of wearable gas sensors largely depend on the flexibility and stretchability of the sensor substrate.

As conventional electrode materials, such as metal, are rigid, it is important to suggest new electrode materials or innovative designs for wearable gas sensors. Several works have overcome the rigidity of metal electrodes. Failure of metal electrodes due to large strain can be alleviated by geometrically engineering the electrode formation. Wavy/serpentine [15,16] and crumpled structures [17] have been widely studied for excellent stretchability and minimizing the strain effect. Another approach is to use intrinsic conductors. Conventional thin film electrodes are brittle and solid and easily lose electrical connection when stretched due to crack formation and film delamination. Liquid metal is one of the electrode candidates as they are intrinsically deformable and retain good conductivity while strained [18,19].

Moreover, liquid metal provides the mechanical and electrical requirements to build mechanically deformable sensors [20]. However, using liquid metals requires high costs as there should be a passivation

* Corresponding author.
** Corresponding author.
E-mail addresses: timothypark@dgist.ac.kr (J. Park), limhch@dgist.ac.kr (H. Lim), yehjunwoo@dgist.ac.kr (J. Yea), chaehyun@dgist.ac.kr (C. Ryu), jsi20039@dgist.ac.kr (S.I. Jung), runiajana@dgist.ac.kr (R. Jana), kijang@dgist.ac.kr (K.-I. Jang), hkeum@kitech.re.kr (H. Keum), joonkim@dgist.ac.kr (H.J. Kim).

https://doi.org/10.1016/j.rineng.2024.101805
Received 25 October 2023; Received in revised form 2 January 2024; Accepted 15 January 2024
Available online 19 January 2024

fabrication process for biosafety issues. Ag nanowires (NW) are also used for stretchable electronics and can be coated via rather simple spray coating and electrospinning. However, Ag NWs have low stretchability and cannot withstand large deformations [21]. The aforementioned conducting materials generally possess a trade-off between stretchability and electrical stability. Therefore, there is much need to develop a novel approach to configuring electrodes in stretchable gas sensors.

Sensing materials should be carefully selected to ensure stable gas detection while maintaining the flexible and stretchable nature of the sensor substrates. Carbon-based nanomaterials have been widely explored owing to room temperature sensing ability and unique electrical and mechanical properties [22–24]. Particularly, carbon nanotubes (CNTs) have drawn much attention for flexible and stretchable gas sensors [25] as they can be deposited on flexible and stretchable substrates via a simple immersion coating method [26]. CNTs exhibit excellent gas sensing ability due to their semiconducting properties and high surface area. Additionally, chemically functionalized CNT-based gas sensors have been studied to address reusability and selectivity [23,27,28]. For example, nanostructured metal oxide materials, such as SnO_2 [29], WO_3 [30], ZnO [31], In_2O_3 [32], and TiO_2 [33], have been reported to be candidates for novel semiconducting gas sensors. TiO_2 is a well-known functional material since it works as a photocatalyst [34,35], accelerating the recovery time of gas sensors at room temperature.

Although the components mentioned above are configured harmoniously with flexible and stretchable sensors, electrical resistance severely changes when stretching the devices. For conventional gas sensors, interdigitated electrode (IDE) structures have been generally utilized due to the high contact area and intact sensing materials [36,

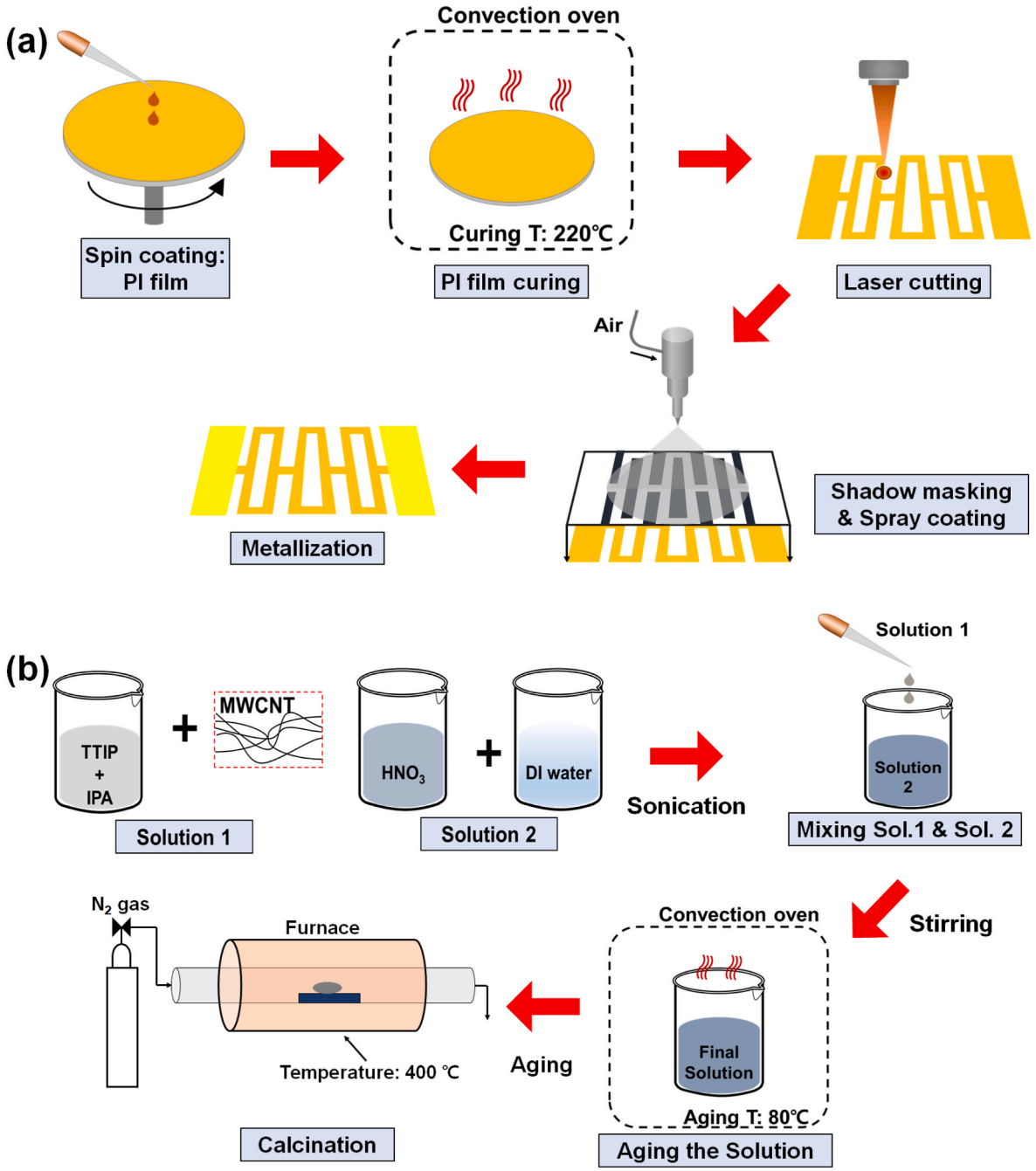

Fig. 1. (a) Fabrication process including PI film spin coating and curing, laser cutting, a spray coating, and the metallization step. (b) Sol-gel synthesis process for TiO_2 functionalization.

37]. However, when IDE-based gas sensors are strained up to 50 %, the electrical conductance dramatically decreases [20]. Various unique architectures have been proposed to minimize the strain effect, such as mogul [38] and 3D-micropatterned PDMS structures [39]. However, they still show a significant increase in resistance change under strain. Such strain-dependent modulation of sensor resistance is inevitable, yet it needs to be studied as the reliability and stability of flexible and stretchable gas sensors are crucial.

The present work introduces Kirigami structure-based CNT gas sensors to address the mechanical deformation effect and validate chemical functionalization on CNTs for gas sensing performance. As the Kirigami structure, inspired by Japanese traditional paper cutting art, is one of the new classes for easily deformable and adjustable frameworks, it can be applied to various emerging flexible and stretchable gas sensing platforms. Specifically, it can minimize stress localization by applying uniaxial strain. In addition, we demonstrate the TiO_2 functionalization to improve further sensing performances, namely measurement sensitivity and response/recovery time. Through unique design and functionalization, we analyze the dependency of sensing parameters of gas sensors as a function of strain. Our results show that effective sensor design is important for developing flexible and stretchable gas sensors.

2. Experimental section

2.1. Device fabrication

Fig. 1(a) depicts the fabrication process of Kirigami structure-based sensors. First, the process begins with spin-coating (SPIN-3000D, MIDAS SYSTEM, Korea) of polyimide (PI) liquid (VTEC PI-1388, STANDARD SYSTEM) to achieve a 50-μm-thick PI film. The spin-coating process is set at a speed of 300 RPM with an acceleration of 5 s for the initial 10 s of spinning, followed by another spin at 500 RPM for 60 s. Setting the acceleration time is crucial to effectively spread the PI liquid on the sacrificial substrate due to its high viscosity. It is soft-baked at 150 °C for 5 min to remove any solvent.

Following the first baking process, PI film is cured at 150 °C for 30 min, and another curing is implemented at 220 °C for 4 h. The cured PI film is then Kirigami-patterned using a carbon dioxide (CO_2) laser cutting machine (VLS4.60, Universal Laser System, USA). To eliminate dirt caused by laser cutting processing, Kirigami patterned PI substrates are thoroughly rinsed with an isopropyl alcohol (IPA) solution. Subsequently, sensing material immersion, bare MWCNT, and TiO_2 functionalized MWCNT are spray-coated at the air flow rate of 0.15 mL/s for 2 min with a shadow mask. Additionally, a 100-nm-thick gold layer is sputter-deposited on each side of the device to form conducting contact pads for wiring. Each unit frame of the Kirigami structure is $2 \times 10\ mm^2$, and the distance between each side of the gold electrodes is 12 mm.

2.2. Materials preparation

Functionalizing metal oxide materials on CNT strongly contributes to its gas-sensing performance [40,41]. Particularly, TiO_2 is one of the well-known metal oxide materials for gas sensing applications and can be synthesized through a rather simple sol-gel process [42,43]. Fig. 1(b) shows the overall process of sol-gel synthesis. Before the synthesis process, 2g of MWCNT powder (Diameter: 8–13 nm, Length: 50∼150 μm, JEIO, Korea) should be acid-treated to make functional groups on CNT outer walls, such as hydroxyl, carboxyl, and carbonyl groups [44] owing to ester bonding formation [45] between TiO_2 and CNT. MWCNT is boiled in 100 mL of 70 % aqueous nitric acid (HNO_3 Sigma-Aldrich, USA) at 80 °C for 6 h with moderate stirring. This functionalized CNT powder is washed with DI water several times to remove acid residuals and dried above 100 °C in the convection oven. The acid-treated CNT is characterized using a Fourier Transform Infrared Spectroscopy (FT-IR, Thermo Scientific/Nicolet Continuum, USA).

1:10 mass ratio of the purchased titanium (IV) isopropoxide (TTIP, Sigma-Aldrich, USA) and IPA solution are mixed, followed by adding acid-treated CNT to make 0.2 wt% CNT solution 1, as shown in Fig. 1(b) [42]. For solution 2, HNO_3 and DI water are mixed until it reach pH 2. Next, solution 1 is added dropwise to solution 2 while vigorously stirring. The resulting colloidal solution is stirred continuously for 2 h to form a sol. Following such a sol formation, the final solution is aged for 24 h in an ethylene glycol bath at 80 °C and exposed to air for another 24 h at ambient temperature to produce a gel. The final samples are then calcined to obtain the crystalline structure of TiO_2 [46] in the furnace at 400 °C for 2 h. For the characterization of TiO_2, we have utilized a Raman spectrometer (Nanobase XperRAM, Korea) and an X-ray Diffractometer (XRD, Malvern Panalytical/Empyrean, UK).

2.3. Gas sensing experiment

Fig. 2 shows the experimental setup for nitrogen dioxide gas sensing. The experiment is performed inside the vacuum probe station with dry nitrogen (N_2) and nitrogen dioxide (NO_2) gases introduced at room temperature. The chamber pressure is maintained at around 660 mTorr using a purge valve controller. The gas flow rate of 100 sccm with 20 ppm NO_2 concentration (N_2 80 sccm, N_2/NO_2 20 sccm) is introduced, while the characterization of various NO_2 concentrations is carried out under changing gas flow rates. Furthermore, the Kirigami structure-based sensor is placed above the surface to exclude the effect of any conduction heat transfer. To recover the sensors, ultraviolet (UV) illumination is employed as it is an efficient method for TiO_2 functionalized CNT gas sensors. NO_2 sensing time is implemented in 7 min. During the NO_2 gas sensing experiment, the electrical resistance of the sensors is recorded every 500 ms.

3. Results and discussion

The functional groups on CNT walls accomplish chemical bonding between CNT and TiO_2. Thus, the purchased CNT powder is needed to be acid-treated using 70 % aqueous HNO_3. Fig. 3(a) represents FT-IR spectra for pristine CNT (P.CNT) and acid-treated CNT (A.CNT) powders. Both powders show peaks ranging from 1992 to 2119 cm^{-1}, originating from CNT [47]. For A.CNT powder, functional groups are confirmed by a peak of C–O, C=OH, and C=O stretching at a broad band below 2000 cm^{-1} [48,49]. Furthermore, O–H stretching vibration in the 3200∼3600 cm^{-1} range is shown due to hydroxyl groups [48].

To investigate the crystalline structure of TiO_2 and differentiate its types, the synthesized TiO_2 is characterized using XRD and Raman spectra, as shown in Fig. 3(b–c). The characteristics peaks of the anatase TiO_2 phase (25°, 48°, 55°, 62°,68°, and 70°) are present [50,51], which is favorable for photocatalytic operation compared to other phases [52]. Fig. 3(c) shows the Raman spectroscopy at room temperature for TiO_2 decorated CNT (T.CNT) and pristine CNT (P.CNT) samples. The peaks at 149, 391, 519, and 640 cm^{-1} represent Raman active vibrations (E_g, B_{1g}, A_{1g}, and E_g, respectively), 1346, 1580, and 2673 cm^{-1} represent the major peaks of CNT corresponding to D, G, and 2D peaks respectively. Fig. 3(d) represents X-ray photoelectron spectroscopy (ESCALAB 250Xi, Thermo Fisher Scientific, US) of the T.CNT composite. Specifically, oxygen-containing C–O functional groups at 286.6eV are detected on the CNT surface, which works for ester bonding formation [53]. Furthermore, the high resolution of anatase TiO_2 particles at 465.2eV and 459.5eV with symmetry can be attributed to Ti $2p_{1/2}$ and Ti $2p_{3/2}$, respectively [54,55]. Transmission electron microscope (TEM, Thermo Fisher Scientific, US) micrographs also confirm that TiO_2 particles are well decorated on CNT outer walls by ester chemical bonding, as shown in Fig. 3(e). Fig. 3(f) shows scanning electron microscope (SEM, Hitachi/SU8020, Japan) micrographs and the elemental coloring mapping via energy-dispersive X-ray spectroscopy (EDS). Elementals mapped in upper Fig. 3(f) correspond to pristine carbon in P·CNT. In the case of T.CNT samples, all the elements, such as carbon, oxygen, and titanium, are well present in a wide raster of samples, as shown in below Fig. 3(f).

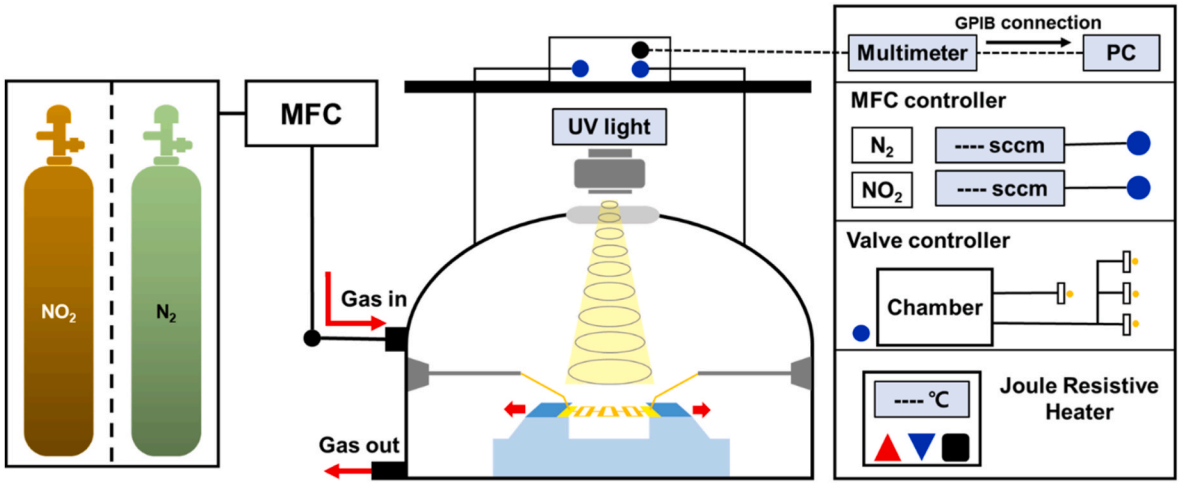

Fig. 2. Experimental setup for nitrogen dioxide gas detection with stretching Kirigami structured gas sensors. UV illumination is implemented while measuring the sensor resistance across the GPIB connection.

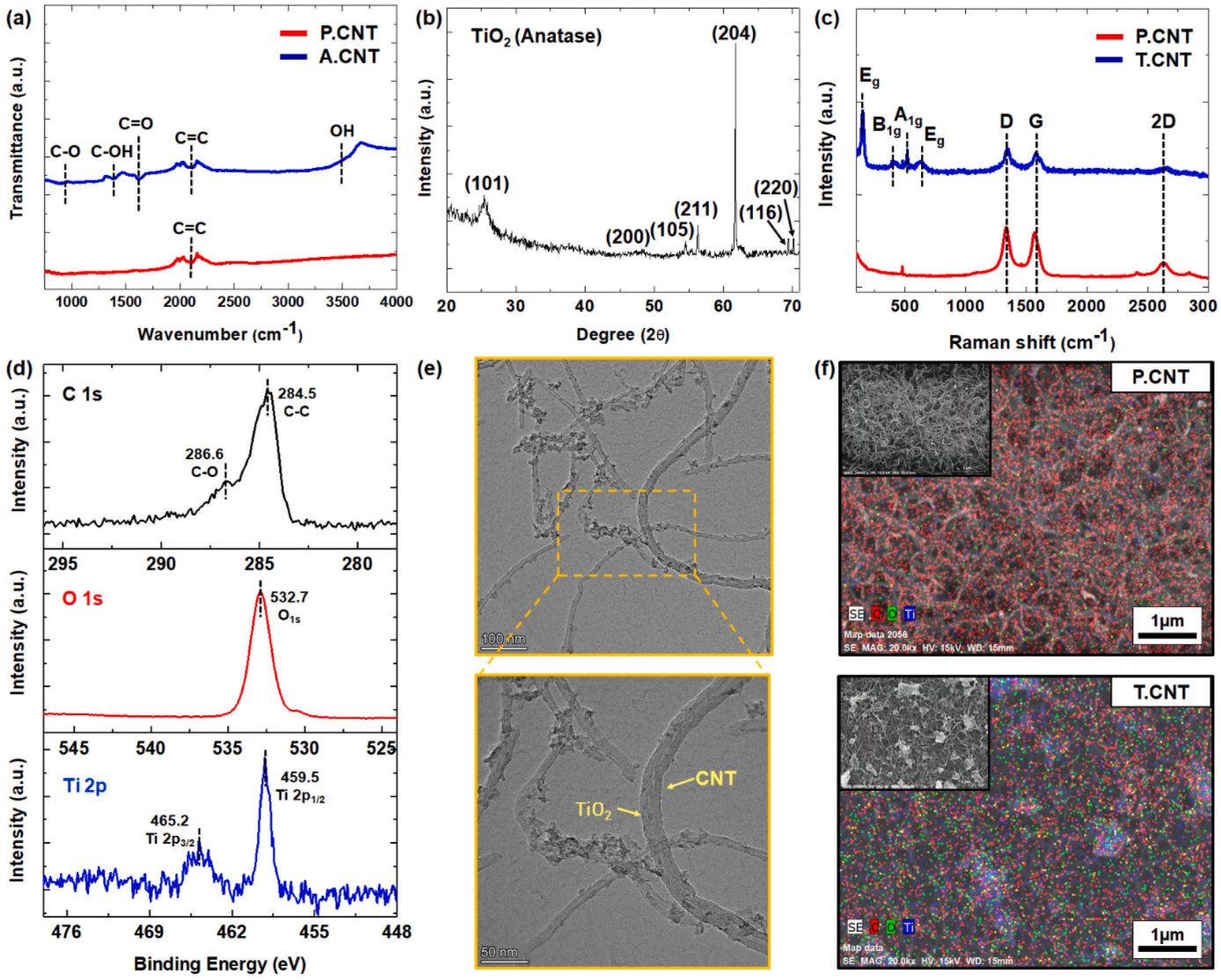

Fig. 3. (a) FT-IR characterization and comparison between pristine CNT (P.CNT) and acid-treated CNT (A.CNT). (b) XRD analysis of anatase TiO_2. (c) Raman analysis of pristine CNT (P.CNT) and TiO_2 decorated CNT (T.CNT). (d) XPS characterization of T.CNT. (e) TEM and (f) SEM micrographs and elemental color mapping of EDS for P.CNT and T.CNT. (For interpretation of the references to color in this figure legend, the reader is referred to the Web version of this article.)

Fig. 4(a) demonstrates stretchability in serial-connected Kirigami devices. The employed Kirigami structure follows a traditional and widely adopted design. Specifically, our design falls into the category of ribbon Kirigami, utilizing cut-only techniques and comprising interconnected void rectangles [56], as illustrated in Fig. S1 in the Supplementary Material. Moreover, this metastructure, inspired by ribbon-type Kirigami, exhibits remarkable properties, including a stiffness reduction by a factor of approximately 30 and an increase in

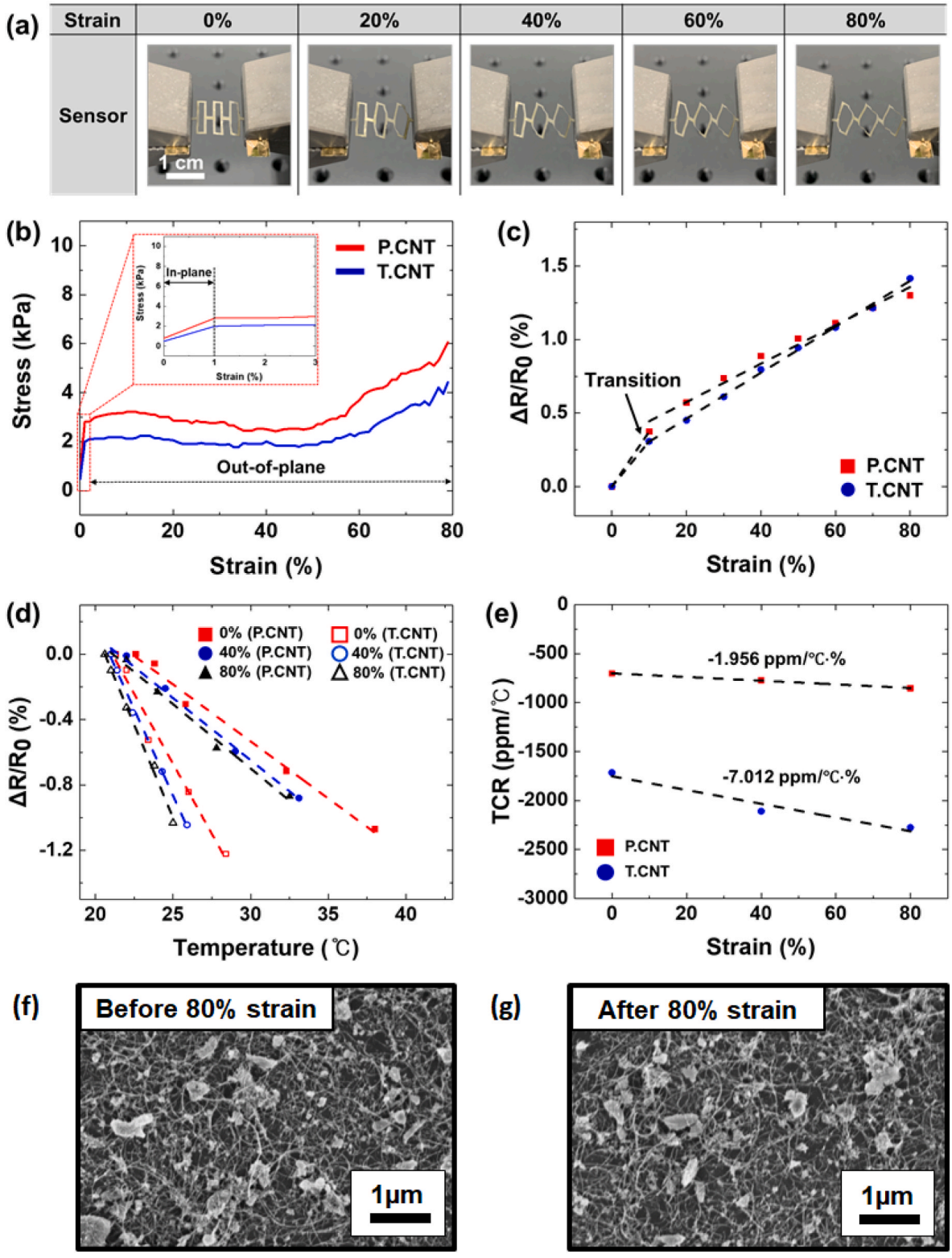

Fig. 4. (a) The digital images of the Kirigami structured sensors as a function of tensile strain ranging from 0 to 80 %. (b) Stress-strain characteristics, and (c) the normalized resistance change with varying the strain for the fabricated sensors. (d) The measured temperature coefficient of resistance (TCR) as a function of tensile strain. (e) TCR comparison between P.CNT and T.CNT while applying the strain. SEM micrographs on T.CNT regions for (f) initial and (g) 80 % stretched state of Kirigami structure.

ultimate strain by a factor of 2 [57]. To begin with the Kirigami mechanism, the initial regime stays in-plane of elementary plates. However, the Kirigami structure starts deforming out-of-plane, accompanied by rotation of certain angles at about 1 % transition strain. Such out-of-plane deformation allows Kirigami patterned substrates to enter the soft regimes [58], and each unit plate of Kirigami patterns uniaxially stretches up to 80 %.

To characterize the mechanical properties of Kirigami patterns, we have measured stress as a function of strain using a dynamic mechanical analyzer (DMA, TA Instruments/DMA850, USA), as shown in Fig. 4(b). Once the Kirigami substrate stretches, there is a small in-plane deformation. However, when it starts twisting at certain angles, it reaches transition and bends out-of-plane, meaning that it has certainly altered from the hard to soft regime. The transition occurs when the energies of the soft and hard regimes become equal [58]. Thus, in a soft regime, stress remains consistent despite applying uniaxial strain. When the deformation localized at the tips of Kirigami patterning exceeds 60 % strain, the structure hardens, and its stress increases again, called the final or third regime. Additionally, the thickness of as-deposited sensing materials is sub-μm, so it does not degrade the device's mechanical properties.

Fig. 4(c) shows the electrical resistance of sensors under strain from

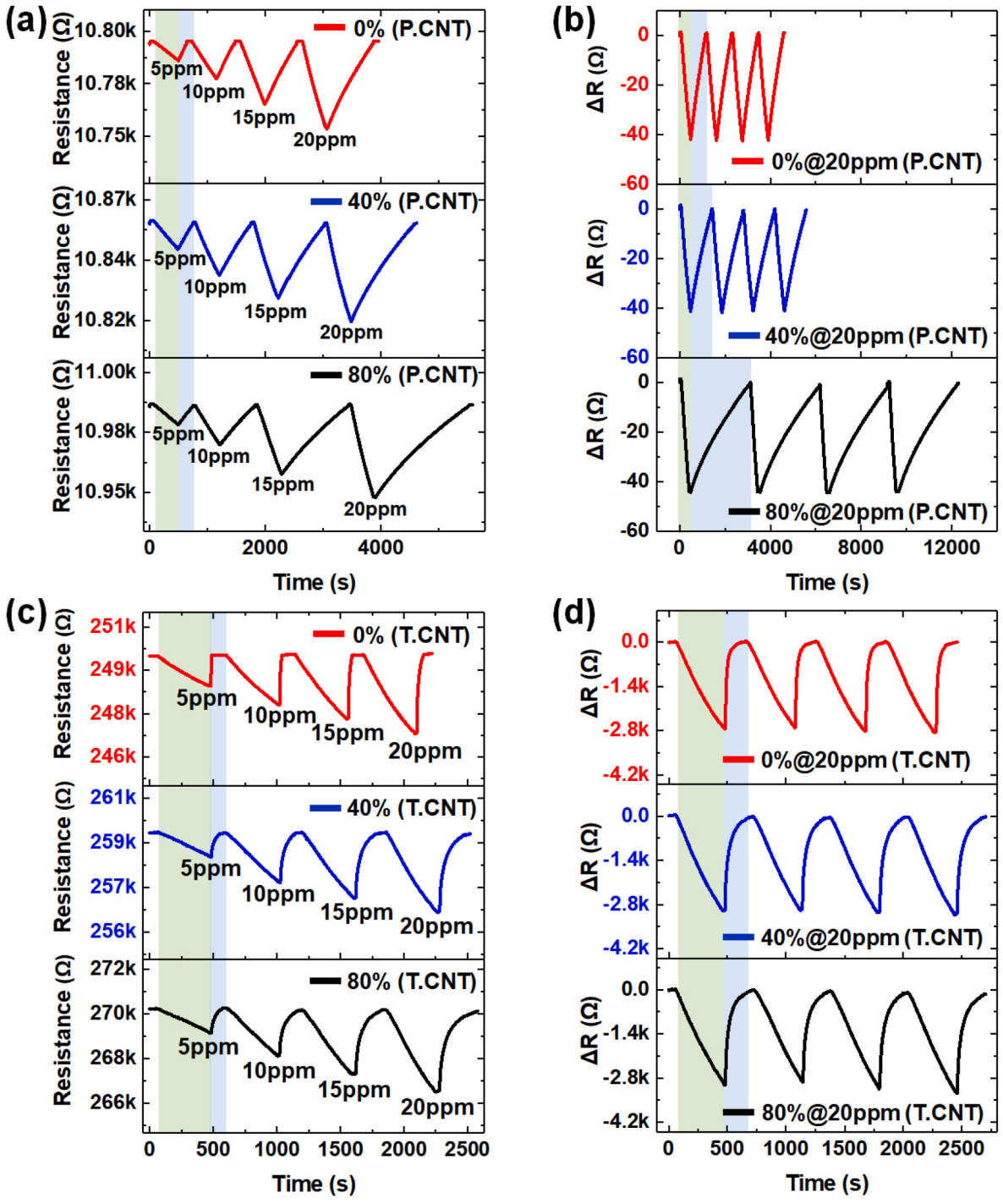

Fig. 5. The electrical sensor resistance with varying NO_2 concentrations at different stretched states, and the change in sensor resistance at 20 ppm fixed NO_2 concentration for 0–80 % strain for (a,b) P.CNT sensors, and (c,d) T.CNT sensors.

0 to 80 %. The measured initial resistance of P.CNT and T.CNT sensors is 10.79 kΩ and 249.77 kΩ, respectively. TiO_2-decorated CNT sensors show higher electrical resistance due to the formation of p-n heterojunctions [59]. However, there is a consistent trend in the normalized change in electrical resistance for both sensors. For example, when they stretch up to 80 %, the normalized resistance change is about 1.3 %. Furthermore, when a Kirigami patterned substrate is deformed to three-dimensional space under the stretching, the bending strain strongly depends on the thickness and bending radius of the Kirigami structured film [60]. Here, the bending strain (ε) is expressed using Equation (1), where d is the film thickness, and R is the bending radius.

$$\varepsilon = d/2R \tag{1}$$

As substrate thickness is proportional to bending strain, it is suggested to control the thickness of substrates to minimize the bending strain affecting the resistance change. Additionally, there is an overall linear dependency in the normalized resistance change at varying uniaxial strains. However, the slopes of the normalized change in resistance for both the sensors alter from 0.03 to 0.015 owing to the softening of Kirigami architecture at transition.

Fig. 4(d) represents the electro-thermal property characterization of the fabricated Kirigami devices as a function of uniaxial strain. Since CNT exhibits p-type semiconducting properties, its temperature coefficient of resistance (TCR) decreases when heated. As we can see from the Figure, the ΔR/R has decreased for T.CNT compared to P.CNT as a whole. It can be attributed to the chemical and heat treatments CNTs undergo in T.CNT instead of the TiO_2, as it behaves as an n-type semiconducting material and would show an opposing trend if taken part. However, TCR is an intrinsic property of the material and varies due to the strain effect [61]. The fabricated Kirigami structure can minimize the change in TCR as a function of strain, as shown in Fig. 4(e). We have carried out the characterization of pre and post-strained sensing material morphologies through SEM images, and it is confirmed that the structure of T.CNT remains consistent without crack formation, as shown in Fig. 4(f and g).

Fig. 5 shows the sensor response as a function of NO_2 gas concentration at strain rates of 0, 40, and 80 %. NO_2 target gas is introduced into the vacuum gas chamber while flowing N_2 purging gas, as indicated in bright green and blue color, respectively in Fig. 5. Fig. 5(a–b) shows the measurement results for P.CNT sensors. In Fig. 5(a), there is a minor increase in initial electrical resistance at each stretched state owing to the distinctive mechanical deformation of the Kirigami structure. It is also observed that the sensor output depends on the NO_2 concentrations. Although the gas sensors are strained up to 80 %, the gas sensing is perfectly carried out as a function of different NO_2 concentrations by utilizing the ultraviolet (UV) light-induced photo desorption method. The 254 nm wavelength UV light source is employed as it is sufficient to detach gas molecules even under the low intensity of 50 μW/cm^2 [62]. For cyclic measurements, the gas detection at 20 ppm NO_2 is implemented, and the equivalent changes of electrical resistance of the P.CNT gas sensors are measured at about 40 Ω regardless of the strain rates.

Under UV illumination, the recovery of the P.CNT sensor differs at different strain rates. Kirigami structure deforms into out-of-plane while stretching, and this mechanical deformation reduces the view factor of UV illumination. Specifically, the UV light source used for recovery is perpendicularly placed above the Kirigami structured gas sensors. As the view factor of UV radiation depends on area, distance, and the angles facing between the surface normals, the view factor of UV radiation significantly decreases, thus increasing the recovery time for largely strained sensors. Although our Kirigami-based P.CNT gas sensors can detect NO_2 at room temperature, the recovery time of sensor resistance and rather low sensitivity need to be addressed.

Fig. 5(c) shows the performance of Kirgiami structured T.CNT gas sensors at various NO_2 gas concentrations. T.CNT gas sensors also exhibit a slight increase in the initial electrical resistance as a function of strain. Fig. 5(d) shows the cyclic gas sensing under 20 ppm of NO_2 of T.CNT sensors at 0, 40, and 80 % strain rates. Compared to unfunctionalized P.CNT sensors, the T.CNT sensors exhibit about tenfold improvement in the recovery time at 80 % strain due to the addition of TiO_2. When UV light illuminates the sensors, the photo-generated holes (h^+) in the valence band diffuse to the TiO_2 surface [63,64]. The holes combine with electrons from NO_2^- (ads) [65], as shown in Equation (3) and (4):

$$h\nu \rightarrow e^- + h^+ \tag{3}$$

$$h^+ + NO_2^-(ads) \rightarrow NO_2(g) \tag{4}$$

Ultimately, it accelerates the NO_2 gas desorption from the sensing material surfaces. This process leaves excessive electrons in the conduction band, reducing the surface's depletion regions. Through this mechanism, the electrical resistance of T.CNT gas sensors returns to the initial resistance within a relatively short time, even though UV light is activated with the lower view factor. As a result, TiO_2 functionalization improved the sensor performances in measurement sensitivity and recovery time.

Fig. 6 summarizes the gas-sensing performance of the fabricated devices. First, the sensitivity (slope) is defined as $(|\Delta R/R_0| \times 100)$/Gas concentration, where R_0 is the initial resistance before detecting NO_2 gas, and ΔR is the change in resistance. To acquire the sensitivity of P.CNT and T.CNT gas sensors, the normalized resistance change as a function of NO_2 gas concentrations is plotted, as shown in Fig. 6(a). The calculated sensitivities from the measurements are about 0.02 %/ppm and 0.05 %/ppm for P.CNT and T.CNT sensors, respectively. T.CNT sensors exhibit about 250 % improvement in the calculated sensitivity compared to P.CNT sensors owing to the heterostructure of CNT and TiO_2 [59]. For example, a depletion region exists at the heterojunction of TiO_2 nanoparticles and CNT, and another is created at the crossing points between two TiO_2-coated CNTs. When the sensors are exposed to NO_2 gas molecules, they are attached to the surface of TiO_2, creating a new depletion region. Then, the adsorbed NO_2 extracts electrons from the TiO_2 due to its highly oxidizing nature, modifying the width of the depletion layer at the surface of TiO_2, altering the depletion layer at the p-CNT/n-TiO_2 junction, thus modifying the sensors' whole resistance.

Furthermore, we define the response at a specific gas concentration using $(\Delta R/R_0) \times 100$. At each cyclic sensing for 20 ppm of NO_2 gas, the responses show no significant differences even under 80 % stretching state for all the sensors, as shown in Fig. 6(b). It is confirmed that our sensors show good reliable, and repetitive measurements under mechanical deformation. Fig. 6(c) exhibits the calculated sensitivities of Kirigami-structured P.CNT and T.CNT sensors as a function of increasing strain. The sensitivities of both sensors remain consistent throughout measurements, meaning that Kirigami structure-based gas sensors are independent of device stretching. In addition, we analyze the limit of detection (LOD) of the developed Kirigami gas sensors using the following Equation [66]: LOD (ppb) = 3 × (R_{rms}/Sensitivity), where 3 is the signal-to-noise ratio, and R_{rms} is root-mean-square (RMS) deviation of baseline signal. We use 120 data points of 1 min for RMS calculation, and the signal-to-noise ratio should be more than 3 due to a valid signal. The calculated LOD from the measurements is about 200 ppb and 100 ppb for P.CNT and T.CNT sensors at all the stretching states, respectively. As the T.CNT gas sensor shows 2.5 times higher sensitivity, and its RMS is fairly stable owing to the Kirigami structure, there is a 200 % improvement in LOD compared to P.CNT sensors.

Additionally, to quantitatively assess the sensor desorption between the fabricated two different sensors, the recovery time of the devices is considered, as shown in Fig. 6(d). Although the attached 20 ppm NO_2 gas molecules are easy to release using UV illumination for P.CNT gas sensors, the recovery time of 80 % strained sensors has quadrupled compared to that of the non-strained ones. It can be explained as follows: when the Kirigami structure stretches up to 80 %, each unit frame of the Kirigami structure becomes significantly bent and twisted. This results in a substantial reduction in the view factor of UV illumination

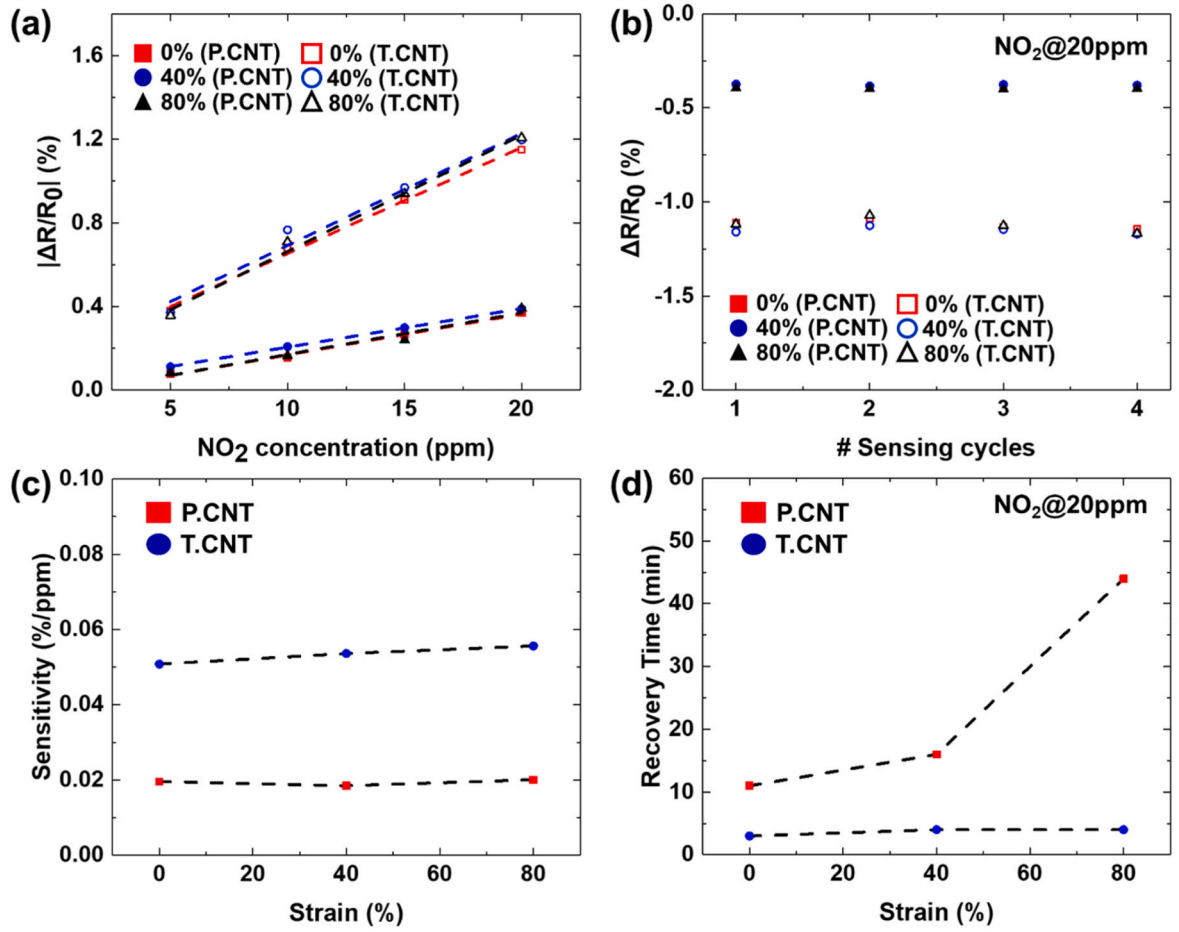

Fig. 6. (a) The absolute normalized change of sensor resistance at varying NO_2 concentrations for all the stretched cases of P.CNT and T.CNT sensors. (b) The variations of sensor response. (c) The sensitivity and (d) the recovery time comparison as a function of strain for all the developed seznsors.

compared to the 40 % strained state. Therefore, it is reasonable to assert that the recovery time of P.CNT sensors exhibits two different recovery rates as a function of strain. However, the functionalization of TiO_2 contributes to a great desorption rate, which corresponds to about 30 s at 10 % of sensor response for all the stretched states. Thus, depending on the target gas or sensor design, a proper functionalization process must be considered for sensor sensitivity and reusability.

The Kirigami gas sensors exhibit stretchable abilities and minor electrical resistance changes. In addition, the TiO_2 functionalization of the sensors improves the measurement sensitivity and desorption rate in NO_2 gas sensing. Table 1 compares the performance of the developed gas sensors to selected previous works on flexible and stretchable gas sensing platforms. The sensor design is one of the crucial factors for developing flexible and stretchable gas sensors. Thus, various types of sensor designs are suggested. For example, serpentine structured sensors use a 60 °C operating temperature. However, they show a long recovery time even at low NO_2 concentrations [67].

Chemical functionalization is essential for high measurement sensitivities and responses [23,38,68–70]. Although the measurement sensitivity or response at a certain gas concentration for our sensors is somewhat limited compared to other functionalized gas sensors, our work dramatically alleviates the inevitable electrical effect from mechanical deformation and exhibits a fast desorption rate compared to previous works. Moreover, it is crucial to consider the impact of humidity on gas-sensing properties due to their potential instability. In humid environments, gas sensors may adsorb water molecules on the sensing material surface [71,72], leading to a degradation in response. Additionally, the interaction between pollutants and various gases could give rise to secondary pollutants [73].

The effect of humidity on the fabricated T.CNT sensor is shown in Fig. S2 in Supplementary Material. Although there is a shift in response under varying humidity conditions, the sensor exhibits a noticeable

Table 1
Summary of flexible and stretchable gas sensors, including the device from this work.

Sensing Materials	Sensor Design	R%@Strain	Sensitivity	Recovery Time	Operating Temperature	Reference
TiO_2/CNT	Kirigami	1.3 %@80 % (Tensile)	0.05 %/ppm (NO_2)	32s@20 ppm	RT	**This work**
MoS_2/rGO	Serpentine	N/A@20 % (Tensile)	7.49 %/ppm (NO_2)	720s@1 ppm	60 °C	[67]
AgNW/Gr	FET	7 %@20 % (Tensile)	5 %@5 ppm (DMMP)	400s@5 ppm	RT	[68]
FGO	Yarn	5 %@0.2 mm (Bending)	12 %@8 ppm(NH_3)	N/A	RT	[69]
Cu/SWCNT	Film	N/A@0.2 mm (Bending)	0.4 %/ppm (H_2S)	20s@20 ppm (RT.)	RT	[23]
R-GO	Mogul pattern	90 %@30 % (Tensile)	2.3 %/ppm (NO_2)	5min@2.5ppm (RT.)	RT	[38]
SnS_2/S-rGO	Film	3 %@Bending 10 %@Twisting	1.32 %/ppm(NH_3)	N/A	RT	[70]

response when exposed to 20 ppm of NO_2. There is an increase in the response ($(\Delta R/R_0) \times 100$) as a function of relative humidity (RH%) levels owing to possible chemical reactions as follows [73]:

$$NO_2\ (g) + e^- \rightarrow NO_2^-\ (ads) \quad (5)$$

$$3NO_2\ (g) + H_2O \rightarrow NO\ (g) + 2HNO_3 \quad (6)$$

$$2NO_2\ (g) + 2NO\ (g) \rightarrow 2NO_3\ (ads) + N_2\ (g) \quad (7)$$

NO_2 gas can be directly adsorbed on the CNT surface owing to its high electron affinity, as shown in reaction (5) [74]. However, NO_2 gas molecules can react with water molecules, leading to the production of HNO_3 in reaction (6) and the formation of functional groups (C=O bonds) on the CNT surface. This enhances reaction (5), and another reaction (7) could be further facilitated. Additionally, oxygen molecules are ionized on the surface of the T.CNT composite to form O_2^- (below 100 °C) and withdraw additional electrons from TiO_2, as shown in the below reaction (8) [75].

$$NO_2\ (g) + O_2^-\ (ads) + e^- \rightarrow 2NO_2^-\ (ads) + O_2 \quad (8)$$

For the comparison of gas selectivity, gases including 20 ppm SO_2, 5 % CH_4, and 5 % H_2 were employed, as illustrated in Fig. S3 in the Supplementary Material. These concentrations were chosen in consideration of the recommended risk concentration levels for each gas [76,77]. The high electron affinity of NO_2, attributed to the presence of lone pairs of holes, surpasses that of other gases, demonstrating excellent selectivity for NO_2 gas. Furthermore, it is anticipated that the integration of appropriate metal oxides [78,79] or novel metals [80,81] onto Kirigami-structured gas sensors could not only ensure stable gas sensing performance but also enable selective gas detection across various gases. However, as sensor reliability and stability relate to the quality of gas sensors, it needs to be further addressed using various approaches, such as the integration of stretchable electrodes or other unique designs. Moreover, to obtain strain-free gas sensors, a significant improvement in sensitivity is required to compensate for the resistance change from mechanical deformation.

4. Conclusion

This paper presents the Kirigami-based CNT gas sensors with TiO_2 functionalization for mechanically deformable capability. The fabrication process carries out a simple spin coating method to control the thickness of the PI film and a laser cutting method for a precise Kirigami structure. In addition, TiO_2 decoration on CNT is implemented via a sol-gel synthesis process for improving the gas sensing performance. The Kirigami architecture exhibits a unique stress-strain relation consisting of three different regimes and considerably mitigates the resistance change despite the applied tensile strain. Following the mechanical and electrical relationship, the electro-thermal properties of P.CNT and T.CNT sensors are characterized. With minor resistance change as a function of increasing strain, stable sensitivities are measured for the developed gas sensors. In addition, TiO_2 functionalization greatly improves the desorption rate at all the stretched states. To make the stretchable sensors more stable and reliable, various reconfigurations of sensor architectures or appliances of stretchable electrodes could be utilized. We envision that our sensors could be applied to wearable and stretchable gas sensing applications beyond NO_2 gas detection.

CRediT authorship contribution statement

Jeonhyeong Park: Writing – original draft, Methodology, Investigation, Conceptualization. **Hyeoncheol Lim:** Investigation, Formal analysis. **Junwoo Yea:** Investigation, Data curation. **Chaehyun Ryu:** Investigation. **Soon In Jung:** Visualization, Investigation. **Runia Jana:** Methodology. **Kyung-In Jang:** Writing – review & editing, Resources. **Hohyun Keum:** Writing – review & editing, Supervision, Resources. **Hoe Joon Kim:** Writing – review & editing, Supervision, Funding acquisition.

Declaration of competing interest

The authors declare that they have no known competing financial interests or personal relationships that could have appeared to influence the work reported in this paper.

Data availability

Data will be made available on request.

Acknowledgment

This work is supported by the National Research Foundation of Korea (NRF-2021R1C1C1011588), funded by the Ministry of Science and ICT of Korea. H.J. Kim thanks the support of the support of the Ministry of Trade, Industry & Energy (RS-2023-00231350). H. Keum thanks the support of the Ministry of Trade, Industry & Energy(MOTIE, Republic of Korea) for “Development of a wearable device and service platform for spa facilities (KM230114)”, and the support of the Korea Institute of Industrial Technology as “Development of core technology for smart sensing and digital medical process to support medical surgical field diagnosis” (KITECH EH-23-0014)”

Appendix A. Supplementary data

Supplementary data to this article can be found online at https://doi.org/10.1016/j.rineng.2024.101805.

References

[1] T.Q. Trung, N.E. Lee, Flexible and stretchable physical sensor integrated platforms for wearable human-activity monitoringand personal healthcare, Advanced materials 28 (2016) 4338–4372.
[2] E. Singh, M. Meyyappan, H.S. Nalwa, Flexible graphene-based wearable gas and chemical sensors, ACS Appl. Mater. Interfaces 9 (2017) 34544–34586.
[3] H.R. Lim, H.S. Kim, R. Qazi, Y.T. Kwon, J.W. Jeong, W.H. Yeo, Advanced soft materials, sensor integrations, and applications of wearable flexible hybrid electronics in healthcare, energy, and environment, Adv. Mater. 32 (2020) 1901924.
[4] K.J. Choi, H.W. Jang, One-dimensional oxide nanostructures as gas-sensing materials: review and issues, Sensors 10 (2010) 4083–4099.
[5] S. Guo, D. Yang, S. Zhang, Q. Dong, B. Li, N. Tran, et al., Development of a cloud-based epidermal MoSe2 device for hazardous gas sensing, Adv. Funct. Mater. 29 (2019) 1900138.
[6] M.K. Smith, K.A. Mirica, Self-organized frameworks on textiles (SOFT): conductive fabrics for simultaneous sensing, capture, and filtration of gases, J. Am. Chem. Soc. 139 (2017) 16759–16767.
[7] R.K. Mishra, A. Barfidokht, A. Karajic, J.R. Sempionatto, J. Wang, J. Wang, Wearable potentiometric tattoo biosensor for on-body detection of G-type nerve agents simulants, Sensor. Actuator. B Chem. 273 (2018) 966–972.
[8] Y. He, M. Zhou, M. Mahmoud, X. Lu, G. He, L. Zhang, et al., Multifunctional wearable strain/pressure sensor based on conductive carbon nanotubes/silk nonwoven fabric with high durability and low detection limit, Adv. Compos. Hybrid Mater. 5 (2022) 1939–1950.
[9] D.M. Correia, S. Ribeiro, A. da Costa, C. Ribeiro, M. Casal, S. Lanceros-Mendez, et al., Development of bio-hybrid piezoresistive nanocomposites using silk-elastin protein copolymers, Compos. Sci. Technol. 172 (2019) 134–142.
[10] X. Xu, S. Wu, J. Cui, L. Yang, K. Wu, X. Chen, et al., Highly stretchable and sensitive strain sensor based on polypyrrole coated bacterial cellulose fibrous network for human motion detection, Compos. B Eng. 211 (2021) 108665.
[11] K.A. Mirica, J.G. Weis, J.M. Schnorr, B. Esser, T.M. Swager, Mechanical drawing of gas sensors on paper, Angew. Chem. Int. Ed. 51 (2012) 10740–10745.
[12] H. Liu, M. Li, O. Voznyy, L. Hu, Q. Fu, D. Zhou, et al., Physically flexible, rapid-response gas sensor based on colloidal quantum dot solids, Adv. Mater. 26 (2014) 2718–2724.
[13] H. Zhao, X. Lin, R. Qi, J. Dai, S. Liu, T. Fei, et al., A composite structure of in situ cross-linked poly (ionic liquid) s and paper for humidity-monitoring applications, IEEE Sensor. J. 19 (2018) 833–837.
[14] R. Ghosh, A. Singh, S. Santra, S.K. Ray, A. Chandra, P.K. Guha, Highly sensitive large-area multi-layered graphene-based flexible ammonia sensor, Sensor. Actuator. B Chem. 205 (2014) 67–73.

[15] G. Li, X. Wu, D.-W. Lee, A galinstan-based inkjet printing system for highly stretchable electronics with self-healing capability, Lab Chip 16 (2016) 1366–1373.
[16] D.S. Gray, J. Tien, C.S. Chen, High-conductivity elastomeric electronics, Adv. Mater. 16 (2004) 393–397.
[17] J. Zang, S. Ryu, N. Pugno, Q. Wang, Q. Tu, M.J. Buehler, et al., Multifunctionality and control of the crumpling and unfolding of large-area graphene, Nat. Mater. 12 (2013) 321–325.
[18] Y. Lin, O. Gordon, M.R. Khan, N. Vasquez, J. Genzer, M.D. Dickey, Vacuum filling of complex microchannels with liquid metal, Lab Chip 17 (2017) 3043–3050.
[19] M.D. Dickey, Stretchable and soft electronics using liquid metals, Adv. Mater. 29 (2017) 1606425.
[20] T.Q. Trung, A. Hanif, S. Siddiqui, E. Roh, W. Lee, N.-E. Lee, A stretchable and highly sensitive chemical sensor using multilayered network of polyurethane nanofibres with self-assembled reduced graphene oxide, 2D Mater. 4 (2017) 025062.
[21] B. Wang, A. Thukral, Z. Xie, L. Liu, X. Zhang, W. Huang, et al., Flexible and stretchable metal oxide nanofiber networks for multimodal and monolithically integrated wearable electronics, Nat. Commun. 11 (2020) 2405.
[22] B. Cho, J. Yoon, S.K. Lim, A.R. Kim, D.-H. Kim, S.-G. Park, et al., Chemical sensing of 2D graphene/MoS2 heterostructure device, ACS Appl. Mater. Interfaces 7 (2015) 16775–16780.
[23] M. Asad, M.H. Sheikhi, M. Pourfath, M. Moradi, High sensitive and selective flexible H2S gas sensors based on Cu nanoparticle decorated SWCNTs, Sensor. Actuator. B Chem. 210 (2015) 1–8.
[24] A. Hanif, A. Bag, A. Zabeeb, D.B. Moon, S. Kumar, S. Shrivastava, et al., A skin-inspired substrate with spaghetti-like multi-nanofiber network of stiff and elastic components for stretchable electronics, Adv. Funct. Mater. 30 (2020) 2003540.
[25] A. Gusain, Carbon Nanotube Based Wearable Room Temperature Gas Sensors, Functional Nanomaterials, Springer, 2020, pp. 329–348.
[26] Z. Gao, Z. Lou, S. Chen, L. Li, K. Jiang, Z. Fu, et al., Fiber gas sensor-integrated smart face mask for room-temperature distinguishing of target gases, Nano Res. 11 (2018) 511–519.
[27] M. Asad, M.H. Sheikhi, Highly sensitive wireless H2S gas sensors at room temperature based on CuO-SWCNT hybrid nanomaterials, Sensor. Actuator. B Chem. 231 (2016) 474–483.
[28] L. Li, C. Fu, Z. Lou, S. Chen, W. Han, K. Jiang, et al., Flexible planar concentric circular micro-supercapacitor arrays for wearable gas sensing application, Nano Energy 41 (2017) 261–268.
[29] M. Inaba, T. Oda, M. Kono, N. Phansiri, T. Morita, S. Nakahara, et al., Effect of mixing ratio on NO2 gas sensor response with SnO2-decorated carbon nanotube channels fabricated by one-step dielectrophoretic assembly, Sensor. Actuator. B Chem. 344 (2021) 130257.
[30] V.T. Duong, C.T. Nguyen, H.B. Luong, D.C. Nguyen, H.L. Nguyen, Ultralow-detection limit ammonia gas sensors at room temperature based on MWCNT/WO3 nanocomposite and effect of humidity, Solid State Sci. 113 (2021) 106534.
[31] R. Saad, A. Gamal, M. Zayed, A.M. Ahmed, M. Shaban, M. BinSabt, et al., Fabrication of ZnO/CNTs for application in CO2 sensor at room temperature, Nanomaterials 11 (2021) 3087.
[32] N. Kohli, A. Hastir, M. Kumari, R.C. Singh, Hydrothermally synthesized heterostructures of In2O3/MWCNT as acetone gas sensor, Sensor Actuator Phys. 314 (2020) 112240.
[33] Y. Seekaew, A. Wisitsoraat, D. Phokharatkul, C. Wongchoosuk, Room temperature toluene gas sensor based on TiO2 nanoparticles decorated 3D graphene-carbon nanotube nanostructures, Sensor. Actuator. B Chem. 279 (2019) 69–78.
[34] Q. Guo, C. Zhou, Z. Ma, X. Yang, Fundamentals of TiO2 photocatalysis: concepts, mechanisms, and challenges, Adv. Mater. 31 (2019) 1901997.
[35] X. Li, Y. Zhao, X. Wang, J. Wang, A.M. Gaskov, S. Akbar, Reduced graphene oxide (rGO) decorated TiO2 microspheres for selective room-temperature gas sensors, Sensor. Actuator. B Chem. 230 (2016) 330–336.
[36] X. Vilanova, E. Llobet, J. Brezmes, J. Calderer, X. Correig, Numerical simulation of the electrode geometry and position effects on semiconductor gas sensor response, Sensor. Actuator. B Chem. 48 (1998) 425–431.
[37] S.P. Lee, Electrodes for semiconductor gas sensors, Sensors 17 (2017) 683.
[38] H.B. Lee, C.W. Bae, L.T. Duy, I.Y. Sohn, D.I. Kim, Y.J. Song, et al., Mogul-patterned elastomeric substrate for stretchable electronics, Adv. Mater. 28 (2016) 3069–3077.
[39] D.-B. Moon, A. Bag, H.-B. Lee, M. Meeseepong, D.-H. Lee, N.-E. Lee, A stretchable, room-temperature operable, chemiresistive gas sensor using nanohybrids of reduced graphene oxide and zinc oxide nanorods, Sensor. Actuator. B Chem. 345 (2021) 130373.
[40] D. Yang, I. Cho, D. Kim, M.A. Lim, Z. Li, J.G. Ok, et al., Gas sensor by direct growth and functionalization of metal oxide/metal sulfide core–shell nanowires on flexible substrates, ACS Appl. Mater. Interfaces 11 (2019) 24298–24307.
[41] S. Vallejos, I. Grácia, O. Chmela, E. Figueras, J. Hubálek, C. Cané, Chemoresistive micromachined gas sensors based on functionalized metal oxide nanowires: performance and reliability, Sensor. Actuator. B Chem. 235 (2016) 525–534.
[42] M. Daraee, M. Baniadam, A. Rashidi, M. Maghrebi, Synthesis of TiO2-CNT hybrid nanocatalyst and its application in direct oxidation of H2S to S, Chem. Phys. 511 (2018) 7–19.
[43] L.A.A. Rodríguez, M. Pianassola, D.N. Travessa, Production of tio 2 coated multiwall carbon nanotubes by the sol-gel technique, Mater. Res. 20 (2017) 96–103.
[44] L. Bazli, M. Siavashi, A. Shiravi, A review of carbon nanotube/TiO2 composite prepared via sol-gel method, Journal of Composites and Compounds 1 (2019) 1–9.
[45] Q. Cao, Q. Yu, D.W. Connell, G. Yu, Titania/carbon nanotube composite (TiO2/CNT) and its application for removal of organic pollutants, Clean Technol. Environ. Policy 15 (2013) 871–880.
[46] M.Z. Yahaya, M.A. Azam, M.A.M. Teridi, P.K. Singh, A.A. Mohamad, Recent Characterisation of Sol-Gel Synthesised TiO2 Nanoparticles, Recent applications in Sol-Gel synthesis, 2017, pp. 109–129.
[47] M. Polyakov, V. Ivanova, D. Klyamer, B. Köksoy, A. Şenocak, E. Demirbaş, et al., A hybrid nanomaterial based on single walled carbon nanotubes cross-linked via axially substituted silicon (IV) phthalocyanine for chemiresistive sensors, Molecules 25 (2020) 2073.
[48] R. Verdejo, S. Lamoriniere, B. Cottam, A. Bismarck, M. Shaffer, Removal of oxidation debris from multi-walled carbon nanotubes, Chem. Commun. (2007) 513–515.
[49] Z. Marković, S. Jovanović, D. Kleut, N. Romčević, V. Jokanović, V. Trajković, et al., Comparative study on modification of single wall carbon nanotubes by sodium dodecylbenzene sulfonate and melamine sulfonate superplasticiser, Appl. Surf. Sci. 255 (2009) 6359–6366.
[50] W.-J. Liou, H.-M. Lin, Nanohybrid TiO2/carbon black sensor for NO2 gas, China Particuol. 5 (2007) 225–229.
[51] M.G. Bhosale, R.S. Sutar, S.B. Deshmukh, M.K. Patil, Photocatalytic efficiency of sol–gel synthesized Mn-doped TiO2 nanoparticles for degradation of brilliant green dye and mixture of dyes, J. Chin. Chem. Soc. 69 (2022) 1730–1743.
[52] T. Luttrell, S. Halpegamage, J. Tao, A. Kramer, E. Sutter, M. Batzill, Why is anatase a better photocatalyst than rutile?-Model studies on epitaxial TiO2 films, Sci. Rep. 4 (2014) 1–8.
[53] X. Wang, X. Li, Y. Zhao, Y. Chen, J. Yu, J. Wang, The influence of oxygen functional groups on gas-sensing properties of reduced graphene oxide (rGO) at room temperature, RSC Adv. 6 (2016) 52339–52346.
[54] L. Zhu, Q. Lu, L. Lv, Y. Wang, Y. Hu, Z. Deng, et al., Ligand-free rutile and anatase TiO 2 nanocrystals as electron extraction layers for high performance inverted polymer solar cells, RSC Adv. 7 (2017) 20084–20092.
[55] W. Hu, Y. Liu, R.L. Withers, T.J. Frankcombe, L. Norén, A. Snashall, et al., Electron-pinned defect-dipoles for high-performance colossal permittivity materials, Nat. Mater. 12 (2013) 821–826.
[56] Y. Sun, W. Ye, Y. Chen, W. Fan, J. Feng, P. Sareh, Geometric Design Classification of Kirigami-Inspired Metastructures and Metamaterials, Structures, Elsevier, 2021, pp. 3633–3643.
[57] D.-G. Hwang, M.D. Bartlett, Tunable mechanical metamaterials through hybrid kirigami structures, Sci. Rep. 8 (2018) 3378.
[58] M. Isobe, K. Okumura, Initial rigid response and softening transition of highly stretchable kirigami sheet materials, Sci. Rep. 6 (2016) 1–6.
[59] C. Marichy, P.A. Russo, M. Latino, J.-P. Tessonnier, M.-G. Willinger, N. Donato, et al., Tin dioxide–carbon heterostructures applied to gas sensing: structure-dependent properties and general sensing mechanism, J. Phys. Chem. C 117 (2013) 19729–19739.
[60] K. Xu, Y. Lu, S. Honda, T. Arie, S. Akita, K. Takei, Highly stable kirigami-structured stretchable strain sensors for perdurable wearable electronics, J. Mater. Chem. C 7 (2019) 9609–9617.
[61] C. Yan, J. Wang, P.S. Lee, Stretchable graphene thermistor with tunable thermal index, ACS Nano 9 (2015) 2130–2137.
[62] R.J. Chen, N.R. Franklin, J. Kong, J. Cao, T.W. Tombler, Y. Zhang, et al., Molecular photodesorption from single-walled carbon nanotubes, Appl. Phys. Lett. 79 (2001) 2258–2260.
[63] B. Pant, M. Park, S.-J. Park, Recent advances in TiO2 films prepared by sol-gel methods for photocatalytic degradation of organic pollutants and antibacterial activities, Coatings 9 (2019) 613.
[64] T. Ueda, K. Takahashi, F. Mitsugi, T. Ikegami, Preparation of single-walled carbon nanotube/TiO2 hybrid atmospheric gas sensor operated at ambient temperature, Diam. Relat. Mater. 18 (2009) 493–496.
[65] D. Nunes, E. Fortunato, R. Martins, Flexible nanostructured TiO2-based gas and UV sensors: a review, Discover Materials 2 (2022) 2.
[66] J. Li, Y. Lu, Q. Ye, M. Cinke, J. Han, M. Meyyappan, Carbon nanotube sensors for gas and organic vapor detection, Nano Lett. 3 (2003) 929–933.
[67] L. Yang, N. Yi, J. Zhu, Z. Cheng, X. Yin, X. Zhang, et al., Novel gas sensing platform based on a stretchable laser-induced graphene pattern with self-heating capabilities, J. Mater. Chem. A 8 (2020) 6487–6500.
[68] W. HyungáCheong, J. HyebáSong, J. JoonáKim, Wearable, wireless gas sensors using highly stretchable and transparent structures of nanowires and graphene, Nanoscale 8 (2016) 10591–10597.
[69] M.-A. Kang, S. Ji, S. Kim, C.-Y. Park, S. Myung, W. Song, et al., Highly sensitive and wearable gas sensors consisting of chemically functionalized graphene oxide assembled on cotton yarn, RSC Adv. 8 (2018) 11991–11996.
[70] Y. Huang, W. Jiao, Z. Chu, S. Wang, L. Chen, X. Nie, et al., High sensitivity, humidity-independent, flexible NO2 and NH3 gas sensors based on SnS2 hybrid functional graphene ink, ACS Appl. Mater. Interfaces 12 (2019) 997–1004.
[71] R. Lontio Fomekong, B. Saruhan, Influence of humidity on NO2-sensing and selectivity of spray-CVD grown ZnO thin film above 400° C, Chemosensors 7 (2019) 42.
[72] B.I. Adamu, A. Falak, Y. Tian, X. Tan, X. Meng, P. Chen, et al., p–p heterojunction sensors of p-Cu3Mo2O9 micro/nanorods vertically grown on p-CuO layers for room-temperature ultrasensitive and fast recoverable detection of NO2, ACS Appl. Mater. Interfaces 12 (2020) 8411–8421.
[73] F. Yao, D.L. Duong, S.C. Lim, S.B. Yang, H.R. Hwang, W.J. Yu, et al., Humidity-assisted selective reactivity between NO2 and SO2 gas on carbon nanotubes, J. Mater. Chem. 21 (2011) 4502–4508.

[74] Y. Wang, L. Liu, F. Sun, T. Li, T. Zhang, S. Qin, Humidity-insensitive NO2 sensors based on SnO2/rGO composites, Front. Chem. 9 (2021) 681313.
[75] B. Zhang, M. Cheng, G. Liu, Y. Gao, L. Zhao, S. Li, et al., Room temperature NO2 gas sensor based on porous Co3O4 slices/reduced graphene oxide hybrid, Sensor. Actuator. B Chem. 263 (2018) 387–399.
[76] R. Kumar, P.K. Kulriya, M. Mishra, F. Singh, G. Gupta, M. Kumar, Highly selective and reversible NO2 gas sensor using vertically aligned MoS2 flake networks, Nanotechnology 29 (2018) 464001.
[77] R. Kumar, N. Goel, M. Kumar, UV-activated MoS2 based fast and reversible NO2 sensor at room temperature, ACS Sens. 2 (2017) 1744–1752.
[78] V.R. Naganaboina, M. Anandkumar, A.S. Deshpande, S.G. Singh, Single-phase high-entropy oxide-based chemiresistor: toward selective and sensitive detection of methane gas for real-time applications, Sensor. Actuator. B Chem. 357 (2022) 131426.
[79] Y. Seekaew, W. Pon-On, C. Wongchoosuk, Ultrahigh selective room-temperature ammonia gas sensor based on tin–titanium dioxide/reduced graphene/carbon nanotube nanocomposites by the solvothermal method, ACS Omega 4 (2019) 16916–16924.
[80] H.S. Lee, J. Kim, H. Moon, W. Lee, Hydrogen gas sensors using palladium nanogaps on an elastomeric substrate, Adv. Mater. 33 (2021) 2005929.
[81] T.-Y. Su, Y.-Z. Chen, Y.-C. Wang, S.-Y. Tang, Y.-C. Shih, F. Cheng, et al., Highly sensitive, selective and stable NO 2 gas sensors with a ppb-level detection limit on 2D-platinum diselenide films, J. Mater. Chem. C 8 (2020) 4851–4858.